Journal of Nuclear Materials 385 (2009) 372–386

Contents lists available at ScienceDirect

Journal of Nuclear Materials

journal homepage: www.elsevier.com/locate/jnucmat

Progress in understanding fission-product behaviour in coated uranium-dioxide fuel particles

M. Barrachin [a,*], R. Dubourg [a], M.P. Kissane [a], V. Ozrin [b]

[a] Institut de Radioprotection et de Sûreté Nucléaire, B.P. 3, 13115 Saint Paul-lez-Durance cedex, France
[b] IBRAE (Nuclear Safety Institute, Russian Academy of Science), Moscow, Russia

ARTICLE INFO

PACS:
28.50.Hw
28.41.Ak

ABSTRACT

Supported by results of calculations performed with two analytical tools (MFPR, which takes account of physical and chemical mechanisms in calculating the chemical forms and physical locations of fission products in UO_2, and MEPHISTA, a thermodynamic database), this paper presents an investigation of some important aspects of the fuel microstructure and chemical evolutions of irradiated TRISO particles. The following main conclusions can be identified with respect to irradiated TRISO fuel: first, the relatively low oxygen potential within the fuel particles with respect to PWR fuel leads to chemical speciation that is not typical of PWR fuels, e.g., the relatively volatile behaviour of barium; secondly, the safety-critical fission-product caesium is released from the urania kernel but the buffer and pyrolytic-carbon coatings could form an important chemical barrier to further migration (i.e., formation of carbides). Finally, significant releases of fission gases from the urania kernel are expected even in nominal conditions.

1. Introduction

In the context of the Generation IV initiative, one particular technology being investigated is the very-high-temperature reactor (VHTR). Based on a helium-cooled, graphite-moderated core, this technology aims to run fuels to very high burn-ups [up to 15 at.% FIMA (Fission per Initial Metal Atom)] and generate high coolant temperatures ($\geqslant$1173 K) [1]. The planned fuel is usually urania (UO_2) (but can also be a mixture of urania and uranium carbide) in the form of sub-millimetric spheres coated with successive layers: a porous carbon coating (the buffer), an inner pyrolytic-carbon coating, a silicon-carbide coating and an outer pyrolytic-carbon coating. These so-called TRISO fuel particles are dispersed in a graphite medium comprising the fuel element.

The UO_2 kernels of TRISO-coated particles present some specificities with respect to UO_2 fuel in pressurized-water reactors (PWRs). These differences are a very much higher fission rate, a significantly higher mean temperature (staying between 1273 and 1473 K in normal operating conditions compared to around 773–1273 K for PWR fuel) that is also fairly homogeneous in the kernel whereas in PWR fuel pellets a significant radial temperature gradient is created. In addition, the targeted burn-up of the TRISO UO_2 fuel kernel is very high (between 10 and 15 at.% FIMA) compared to that of PWRs (around 5 at.% FIMA). One can expect the formation of considerably larger amounts of fission gases (affecting the evolution of the fuel–kernel microstructure) and altered chemical forms of the solid fission products (FPs) due to the high temperature and the different evolution of the oxygen potential within the carbon-coated UO_2 kernel. This latter difference arises when, as part of the fission process, some of the oxygen liberated from the UO_2 fuel kernel combines with the carbon of the surrounding porous buffer layer to form CO and/or CO_2 [2]. This, in addition, may induce extra mechanical stresses in the particle due to pressurization which can, in turn, impact the FP behaviour.

These physical and chemical phenomena are today under investigation (e.g., within the European RAPHAEL Project [3]) since they may lead to many important modifications affecting the fuel performance during normal or off-normal operation, e.g., regarding the kernel size (swelling), the stresses in the coatings (particle pressurization due to fission gases and carbon oxides), the corrosion of the coating layers by some FPs [4], etc. Nonetheless, some of these wide-ranging and complex phenomena occurring during irradiation of oxide fuels have been studied for a long time in light-water reactors (e.g. [5]). Application of this knowledge to TRISO particles may provide significant insights into FP behaviour in these particles and the evolution of the kernel microstructure for which there are very few available experimental data.

Hence, in this paper, two mechanistic approaches (MFPR [6], *Module for Fission-Product Release*, and MEPHISTA [7], *Multiphase Equilibria in Fuels via Standard Thermodynamic Analysis*), originally developed for PWR studies by the French 'Institut de Radioprotection et Sûreté Nucléaire' in close collaboration with the Russian Nuclear Safety Institute (IBRAE) and the THERMODATA/CNRS/INPG

* Corresponding author. Tel.: +33 4 42 19 94 14; fax: +33 4 42 19 91 67.
E-mail address: marc.barrachin@irsn.fr (M. Barrachin).

0022-3115/$ - see front matter © 2008 Elsevier B.V. All rights reserved.
doi:10.1016/j.jnucmat.2008.12.025

Laboratory, are used to analyse TRISO particles. MFPR is a computer code mechanistically modelling FP behaviour in irradiated UO_2 fuel in normal and accident situations. It describes the evolution of the various defects of the fuel microstructure and their interaction with fission-gas atoms and bubbles. The model also includes the chemistry of FPs in the temperature range 500–3000 K by considering the chemical equilibrium at the grain boundary of the multicomponent and multiphase U–O–FP system. MEPHISTA is a self-consistent non-ideal-solution database designed for thermochemical equilibria calculations. Initially created for UO_2 and MOX fuels, it has recently been extended to next-generation nuclear fuels by including carbon and silicon (and their compounds) as chemical elements. The CALPHAD approach [8] is used to obtain the assessed parameters of the Gibbs energies of all the phases in the chemical system Ba–C–Cs–La–Mo–O–Pu–Ru–Si–Sr–U–Zr + Ar–H.

In the past, the approaches applied to predict FP behaviour in TRISO particles were mainly based on thermodynamic calculations (e.g. [9–11]). In such evaluations, kinetic aspects (such as solid-state diffusion) which may be important in the temperature regime of interest for the VHTR design are obviously not taken into account. For this reason, the simultaneous application here of kinetic and thermodynamic approaches appears to be original and, above all, complementary. Indeed, it allows detailed treatment of the thermodynamic system presented by the particle (associating UO_2, FPs and carbon from the buffer layer), a system in which one assumes that each element can react with all others (i.e., the equilibrium hypothesis without kinetic considerations), and the dynamic processes of FP migration, accumulation, formation of separate phases and microstructure evolution within the fuel kernel (the MFPR approach).

Supported by results of calculations performed with both tools, this paper presents an investigation of some important aspects of the fuel microstructure and chemical evolutions of irradiated TRISO particles. This analysis has been performed by comparing and contrasting the very few known experimental studies involving measurements made on irradiated TRISO fuel, in particular from Minato et al. [9], with calculated results.

2. Oxygen potential and particle pressurization

It is usually assumed that the fission of uranium atoms (i.e., the burn-up) causes the oxygen potential of the fuel to increase [12]. In this way, during irradiation the fuel is assumed to become slightly hyperstoichiometric even if this evolution is tempered for TRISO fuel by the reaction of some of this oxygen with the carbon of the buffer layer. The resulting formation of carbon monoxide and dioxide gases acts to pressurize the particle adding to the internal pressurization from fission gases. This effect obviously increases with burn-up. It may lead, in extreme conditions, to the failure of the particle. For this reason, the determination of the CO, CO_2 and FP (in particular Xe and Kr) contributions to the internal pressure is critical in predicting the thermomechanical behaviour of the particles in nominal or accidental conditions.

To this end, equilibrium calculations are performed considering a thermodynamically-closed system comprising the UO_{2+x} kernel, the carbon buffer and a buffer volume (equal to 3×10^{-11} m^3, a volume corresponding to the geometrical characteristics given in [9]). The stoichiometric deviation, x, is used here as a variable parameter representing a variable amount of the fission products. This approach has been chosen rather than performing direct calculations with the FP present in the MEPHISTA database since certain FPs with significant fission yields such as neodymium and cerium are absent in the database where these can significantly alter the evaluation of the oxygen potential and hence the CO and CO_2 pressures. It can be noted that even calculation of the oxygen potential with a complete thermochemical database should also be regarded as approximate given the incomplete knowledge of FP behaviour in the UO_2 kernel. Additionally, the burn-up dependence of the oxygen potential in irradiated fuels remains today an intensely debated point in the literature (see [13,14]). For these reasons, here, the thermodynamic calculations are presented as a function of oxygen potential.

In this frame, the accurate modelling of the U–C–O phase diagram is essential to estimate reliably the CO and CO_2 pressures. The CALPHAD models of the two border sub-systems, U–C and U–O, of the U–C–O phase diagram, published in [15,16], are parts of the MEPHISTA modelling. In particular, the U–O model satisfactorily reproduces the experimental database for oxygen potential in UO_{2+x} that governs the free oxygen over the hyperstoichiometric fuel for the carbonic gas formation. The U–C–O phase diagram is optimised on the basis of the different experimental ternary sections compiled by Potter [17] and completed by the thermodynamic properties of the C–O and U–O gases. It can be shown that the present model fits well the experimental values of CO pressures over U–C–O as recently reviewed in [18].

Fig. 1 provides the respective contributions to the internal pressure in the particle of the carbonic gases (CO and CO_2) at 1450 K and at 1873 K versus the oxygen potential. The chosen temperatures correspond, respectively, to nominal operating conditions and to the design-objective upper-bound temperature in accident conditions for modern HTRs [19]. For both temperatures, CO pressure dominates that of CO_2 for values of oxygen potential below -325 kJ mol^{-1}. Oxygen-potential measurements in irradiated TRISO particle are very scarce. Lindemer and de Nordwall [20] reported calculated oxygen potentials from measurements of CO released from irradiated UO_2-coated particles (6% FIMA) between -480 and -380 kJ mol^{-1} at 1450 K and between -500 and -380 kJ mol^{-1} at 1873 K. The highest value (-380 kJ mol^{-1}), located below the equilibrium oxygen potential of Mo/MoO_2 in the temperature interval 1450–1873 K, is consistent with the microanalyses available in [9] which indicated that, for a slightly lower burn-up (<5.2% FIMA), Mo was mostly present in the metallic precipitates.

At -380 kJ mol^{-1} (maximum value in [20] for 6% FIMA), the sum of CO and CO_2 pressures could reach a maximum of 6 and 23 MPa at 1450 and 1873 K, respectively (Fig. 1). These values are in agreement with the calculations previously performed by Schram et al. [10] or with the evaluations of Minato et al. [9] for the same particle geometry and U, O, C inventories. This pressurization, acting on the silicon carbon layer has to be compared to the maximum pressure (about 100 MPa [20]) equivalent to the ultimate tensile strength, ϕ_{SiC}, of silicon carbide (SiC). For such a moderate burn-up (6% FIMA), the total pressure CO + CO_2 within the coated particle does not attain this critical value either in nominal operations (1450 K) or in accidental conditions (1873 K). The pressure corresponding to ϕ_{SiC} is reached when the oxygen potential is between -330 and -325 kJ mol^{-1}. These values correspond to an oxygen potential in equilibrium with UO_{2+x}, with a specific x which is calculated to be lower than 0.001 (Fig. 2). This result is in agreement with the estimates previously made in [20,21].

Recent measurements [13] have indicated that this oxygen-potential range between -325 and -350 kJ mol^{-1} can be potentially reached for a burn-up of 9% FIMA in PWR UO_2 fuel at 1273 K. For such low-enriched fuel, the burn-up accumulated after the third irradiation cycle mainly results from the fission of ^{239}Pu which is known to be a more oxidising process than the fission of ^{235}U. For the TRISO fuel kernel, the uranium fission is assumed to be preponderant during a longer time considering the higher initial enrichment. Consequently it is expected that TRISO UO_2 kernels reach these oxygen-potential values at higher burn-up.

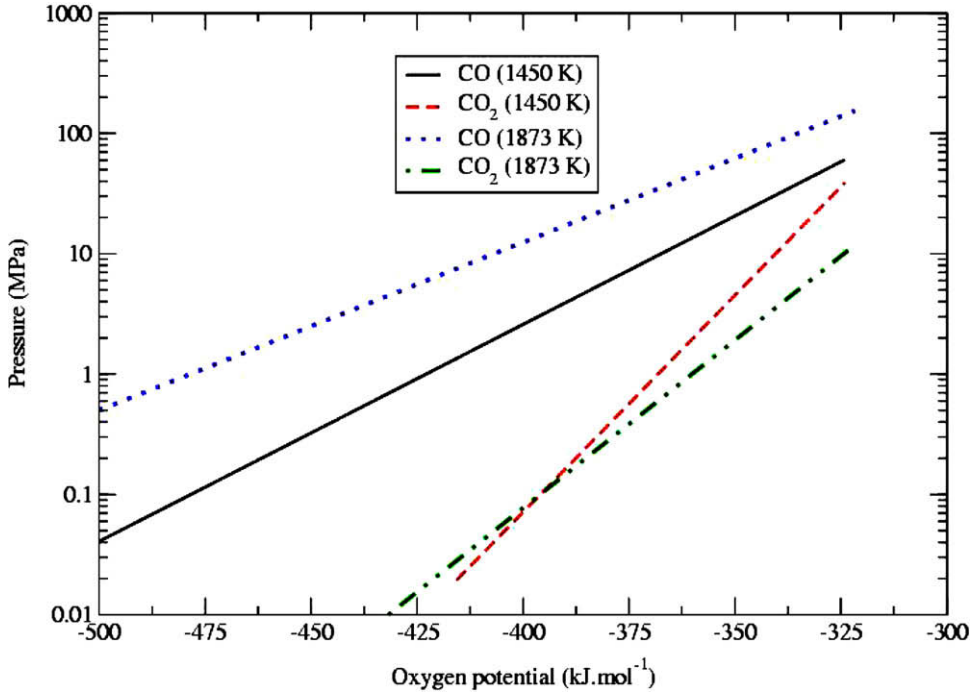

Fig. 1. Thermodynamic calculations of CO and CO_2 pressures in the TRISO particle as a function of oxygen potential at 1450 and 1873 K.

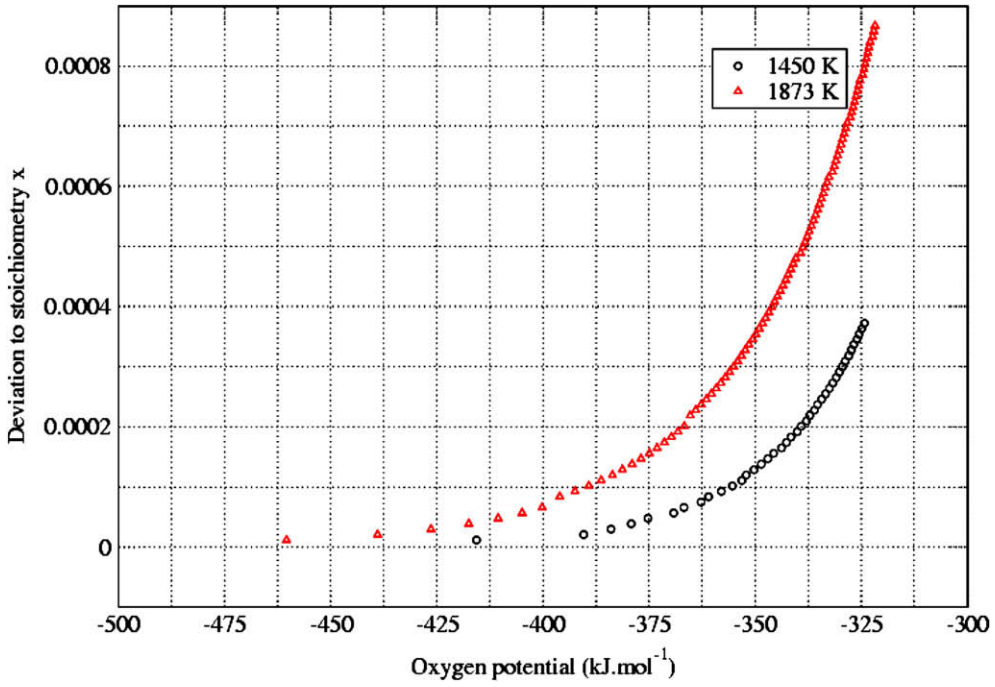

Fig. 2. Calculated x in UO_{2+x} fuel in equilibrium with carbon as a function of oxygen potential at 1450 and 1873 K.

For such a high burn-up (>9% FIMA), an additional but important contribution to the particle pressurization due to fission gas (Xe and Kr) formation has to be taken into account in the calculation of the thermomechanical loading of the particle. At 9% FIMA, the pressures of the fission gases can represent one half of the contribution of CO and CO_2 (Fig. 3). At lower burn-up (e.g. 6% FIMA), it must be stressed that pressurization of the particle should arise principally from fission-gas release. The significant role played by the fission gases on the pressurization of the particle has to be tempered by the fact that the pressure may be lower since some fraction of these noble gases may remain trapped in the fuel kernel. Nevertheless, the MFPR calculations (see below) indicate that significant release of fission gas occurs even at low temperature (e.g., ~20% for 4% FIMA or ~35% for 10% FIMA at 1450 K).

To summarise, the prevalent oxygen potential, while evaluated with some uncertainty, does not lead to excessive pressurization (relative to the ultimate tensile strength of silicon carbide) due

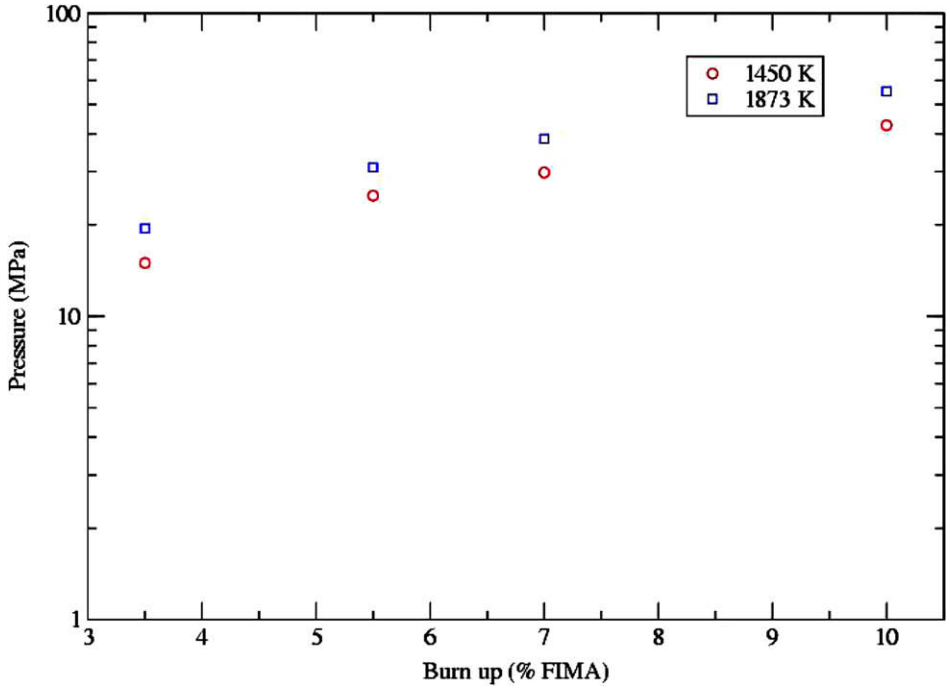

Fig. 3. Thermodynamic calculations of the Xe + Kr pressure as a function of burn-up at 1450 and 1873 K.

to carbon monoxide (or dioxide) formation *up to at least 9% FIMA*. At high burn-up (>9% FIMA, that is foreseen in the design of the actual VHTR), the CO and CO_2 pressures may become an unacceptable loading regarding the mechanical integrity of the particle. It has been recently shown experimentally that the kinetics of formation of CO could limit the build up of the internal pressure of the particle [22]. For this reason, the CO and CO_2 pressure values determined from the equilibrium calculations presented here have to be considered as conservative. Nevertheless, the failure of the SiC layer may happen by other means where CO formation is implied. Corrosion of the SiC layer by CO can occur resulting from failure of the inner pyrolytic-carbon layer caused by an irradiation-induced shrinkage [23]. CO and CO_2 pressures are suspected of being partly responsible for the mechanical weakening of the inner pyrocarbon coating by acting as the vehicle for mass transfer of carbon in presence of a thermal gradient [24]. For these reasons, the suppression of excessive CO formation during oxidation of UO_2 based particle remains an important design objective at moderate and high burn-up.

3. Fuel chemistry

Knowledge of fuel chemistry is an important item for the design of the VHTR particle since it is a prerequisite for the determination of potential release that must be evaluated for normal or accident conditions. The fission-product behaviour also impacts the evolution of the kernel oxygen potential which in turn influences the pressurization of the particle. Finally some fission products released from the kernel might attack the coatings (SiC notably).

The behaviour of chemically active elements, beyond the thermochemical stability of species, depends on temperature, the solubility of elements/oxides in the fuel and the fuel oxygen potential. To determine this behaviour, calculations with both approaches (MEPHISTA and MFPR) are performed. It is worth noting that there are significant differences between these approaches and these are described below.

- MEPHISTA provides an equilibrium composition of a chemical system with a given inventory of chemical elements. Kinetic aspects are therefore not considered. In contrast, MFPR calculates the dynamic processes of FP migration and accumulation at the grain boundaries; formation of compounds and phases is calculated to be at equilibrium at the grain boundaries.
- MEPHISTA calculations are performed at a given value of the oxygen potential while MFPR provides a value of the oxygen potential as a result of a set of oxidation/reduction reactions with oxygen participation considered in a self-consistent manner.
- Regarding the extension of the treated chemical system, the list of the important FPs in the MFPR database is almost complete but the thermodynamic description of the ternary phases (precipitating at the fuel grain boundaries) mostly refers to stoichiometric compounds. In contrast, MEPHISTA provides the thermochemical behaviour of the ternary phases not only as stoichiometric substances but also as solid solutions (where these exist) and allows the impact of carbon to be considered in detail though for a more restricted chemical system in terms of FPs.

For all these reasons, the two approaches appear highly complementary for the investigation of the fuel chemistry of the TRISO particle.

Very few experimental investigations of fuel–kernel chemistry are available. Electron Probe Microanalysis Examinations (EPMA) on irradiated TRISO particles were reported by Minato et al. [9] but the burn-up (about 4–5% FIMA) is relatively modest regarding the objective of the VHTR technology (burn-up >10% FIMA). There are apparently no experimental data relating to fuel chemistry for such high burn-up particles.

In this context, firstly conditions representative of the ranges of the irradiation conditions in terms of burn-up and temperature investigated in [9] were chosen: (A) 1450 K, 120 Effective Full-Power Days, 4% FIMA; (B) 1700 K, 100 Effective Full-Power Days, 4% FIMA. The lowest temperature (1450 K) corresponds to nominal

operating conditions. The highest temperature (1700 K) is somewhat lower than that fixed as a design-objective maximum in an accident (1873 K). However, many of Minato's experimental analyses were performed on particles irradiated at this temperature and can be consequently compared to the calculations.

Secondly, some calculations at higher burn-up (10% FIMA, 1450 K), more relevant to the VHTR technology, are also presented.

For the MFPR calculations, taking into account the size of the fuel kernel (~0.5 mm diameter), homogeneous conditions have been assumed. One must note for example, that in the case of the irradiation experiments in [9], the conditions of irradiation are fairly constant because in many cases the difference between the mean average temperature and the maximum temperature was not very significant (no more than roughly 150 K). This allows, at least in a first approach, the MFPR calculations to be performed considering constant temperature and fission rate.

3.1. Behaviour of fuel (4% and 10% FIMA) at 1450 K and at 1700 K (4% FIMA)

The main results of the MFPR calculation at 1450 K can be summarised as follows (Table 1):

1. Molybdenum is predicted to form mainly metallic precipitates and to a lesser extent molybdate (Cs_2MoO_4).
2. Caesium is mainly trapped in uranate (Cs_2UO_4) and to a lesser extent molybdate (Cs_2MoO_4); CsI (caesium iodine) is also formed.
3. The behaviour of barium and strontium are similar since they form uranates ($BaUO_4$ and $SrUO_4$); strontium is more significantly trapped in the UO_2 solution in agreement with experimental data [25].
4. Practically all zirconium is in the UO_2 matrix and the formation of zirconates is suppressed.

EPMA observations performed by Minato et al. [9] within the fuel kernel did not reveal ternary oxide compounds. In contrast, they confirmed the presence of metallic precipitates (five-metal precipitates, Pd–Te, ...). This clearly indicates that molybdenum was not fully oxidised during irradiation, i.e., in agreement with the MFPR result which additionally provides the value of the oxygen potential, −455 kJ mol^{-1}. This value may appear to be slightly too low in comparison with the oxygen-potential database compiled by Spino et al. [14] for PWR irradiated UO_2 which indicates, for a similar burn-up, a higher value (i.e., >−450 kJ mol^{-1}), even if these values are not directly comparable due to the difference of enrichment between PWR fuel and HTR fuel kernels.

The speciation given by MFPR is then mainly characterised by formation of a large amount of uranate-type phases. This result is very different from the chemical state of FPs as given by the thermodynamic database MEPHISTA which predicts, for an oxygen potential fixed at −455 kJ mol^{-1}, the trapping of barium (and some part of strontium) in the (Ba,Sr)(U,Zr,Mo)O_3 perovskyte phase (the so-called grey phase already identified in some microanalyses of irradiated oxide fuels [26]).

At higher burn-up (10% FIMA, 1450 K), the speciation for FPs given by MFPR does not change significantly (Table 2).

The FP speciation given by MFPR exhibits a significant change at 1700 K for 4% FIMA, i.e., conditions close to those of the Minato et al. tests (Table 3). One can note a reduction of uranate amounts and preferential trapping of barium and strontium in zirconates ($BaZrO_3$ and $SrZrO_3$). The chemical form of caesium is also changed since it is principally found in a molybdate phase (Cs_2MoO_4) whereas it was trapped in uranate (Cs_2UO_4) at lower temperature. This result seems to be more in agreement with what it is expected from the analysis of the thermodynamic stabilities of the different ternary oxide phases [27] which usually shows the preferential formation of Cs_2MoO_4 relative to formation of Cs_2UO_4.

EPMA on the coating layers of the TRISO particles which experienced higher temperatures (1783, 1743 and 1688 K for the S5, S6 and S9 tests in [9], respectively) show that part of the barium and the cerium in oxide forms were located in the buffer layers. Caesium was also detected in the buffer and in the pyro-carbon layers with a homogeneous distribution for the S3 test (5% FIMA, 1773 K). In the MFPR calculations, caesium is released from the kernel but only to a small extent (Table 3). By contrast, in the MFPR

Table 1
Distribution (expressed in%) of Cs, Mo, Ba, Sr, Zr, La in the different phases (4% FIMA, 1450 K) as predicted by MFPR.

	UO_2 solid solution	Metallic phase Ru–Mo–Tc–Rh–Pd	Oxide phases						CsI
			Uranate	Molybdate			Zirconate		
Cs	~2 (Cs)		~62 (Cs_2UO_4)	~30 (Cs_2MoO_4)			0 (Cs_2ZrO_3)		~6
Mo	~2 (MoO_2)	~87		~11 (Cs_2MoO_4)	0 ($BaMoO_4$)	0 ($SrMoO_4$)			
Ba	~2 (BaO)		~91 ($BaUO_4$)	0 ($BaMoO_4$)			~7 ($BaZrO_3$)		
Sr	~9 (SrO)		~90 ($SrUO_4$)	0 ($SrMoO_4$)			~1 ($SrZrO_3$)		
Zr	~98 (ZrO_2)						0 (Cs_2ZrO_3)	~1.8 ($BaZrO_3$)	~0.2 ($SrZrO_3$)
La	100 (La_2O_3)								

Table 2
Distribution (expressed in%) Cs, Mo, Ba, Sr, Zr, La in the different phases (10% FIMA, 1450 K) as predicted by MFPR.

	UO_2 solid solution	Metallic phase Ru–Mo–Tc–Rh–Pd	Oxide phases						CsI
			Uranate	Molybdate			Zirconate		
Cs	~1 (Cs)		~61 (Cs_2UO_4)	~32 (Cs_2MoO_4)			0 (Cs_2ZrO_3)		~6
Mo	~1 (MoO_2)	~86		~13 (Cs_2MoO_4)	0 ($BaMoO_4$)	0 ($SrMoO_4$)			
Ba	~1 (BaO)		~91 ($BaUO_4$)	0($BaMoO_4$)			~8 ($BaZrO_3$)		
Sr	~2 (SrO)		~90 ($SrUO_4$)	0 ($SrMoO_4$)			~8 ($SrZrO_3$)		
Zr	~95 (ZrO_2)						0 (Cs_2ZrO_3)	~2.5 ($BaZrO_3$)	~2.5 ($SrZrO_3$)
La	100 (La_2O_3)								

Table 3
Distribution (expressed in%) Cs, Mo, Ba, Sr, Zr, La in the different phases (4% FIMA, 1700 K) as predicted by MFPR (∗) 0.2 of Cs is released.

	UO_2 solid solution	Metallic phase Ru–Mo–Tc–Rh–Pd	Oxide phases						CsI
			Uranate	Molybdate			Zirconate		
Cs(∗)	∼3.8 (Cs)		∼16 (Cs_2UO_4)	∼74 (Cs_2MoO_4)			0.2 (Cs_2ZrO_3)		∼5.8
Mo	∼4 (MoO_2)	∼69		∼27 (Cs_2MoO_4)	0 ($BaMoO_4$)	0 ($SrMoO_4$)			
Ba	∼4 (BaO)		∼30 ($BaUO_4$)	0 ($BaMoO_4$)			∼66 ($BaZrO_3$)		
Sr	∼10 (SrO)		∼56 ($SrUO_4$)	0 ($SrMoO_4$)			∼34 ($SrZrO_3$)		
Zr	∼75 (ZrO_2)						0 (Cs_2ZrO_3)	∼17 ($BaZrO_3$)	∼8 ($SrZrO_3$)
La	100 (La_2O_3)								

calculations barium as well as cerium is fully trapped in condensed phases in disagreement with the observations.

3.2. Discussion

3.2.1. Strontium and barium behaviour

The main difference between the MFPR speciation and the MEPHISTA thermodynamic calculation is the preferential trapping of barium and some part of the strontium in uranate phases in the MFPR calculations at 1450 K. To explain this difference, one has to investigate the particular role played by zirconium on the fission-product speciation. Indeed, the presence (or absence) of zirconium at the fuel grain boundaries may induce very different forms for some of the FPs. In particular, in the case of sluggish diffusion of zirconium towards the grain boundaries or/and high solubility of zirconium in UO_2, one expects that formation of a uranate-type ternary phase could be favoured instead of zirconates.

It is well known that zirconium dioxide (ZrO_2) is highly soluble in uranium dioxide at high temperature (i.e., >1700 K) [28]. At lower temperature, this solubility strongly decreases where Romberger et al. [28] measured at the eutectoid temperature of the UO_2–ZrO_2 phase diagram (1383 K) a content of 0.38 mol.% of ZrO_2 in UO_2. On this experimental basis, zirconium is assumed, in the thermodynamic models, to precipitate as a separate phase and its presence at the grain boundaries usually results in the preferential formation of zirconate-type compounds since these compounds are more thermodynamically stable than uranates. Nevertheless, it is not excluded that the solubility of zirconium in irradiated UO_2 fuel at low temperature is increased due to the increase of the number of defects created by irradiation. The theoretical work of Grimes and Catlow [29] using a Mott-Littleton simulation technique, calculated slightly positive values for the solution energy of ZrO_2 in $UO_{2\pm x}$ at 0 K indicating that the solution of ZrO_2 in UO_2 is not *a priori* energetically favourable. The solution energy includes a term corresponding to the dissociation of zirconium dioxide. Through this term, this energy is representative of the ability of zirconium dioxide to be soluble in urania as it can be measured in classical thermodynamic experiments (e.g., [28]). In the situation of cations produced inside irradiated fuel, the pertinent energy is more likely the incorporation energy of the cation in the UO_2 matrix in a pre-existing defect. Whatever the defect type in the UO_2 matrix, Grimes and Catlow [29] showed that zirconium solubilisation is always a favourable process from an energetic point of view. The lowest incorporation energy corresponds to the uranium vacancy. It can be shown that the concentration of this defect type strongly increases during the irradiation process (MFPR calculation in Fig. 14). In the case of very-low thermodynamic solubility such as that of zirconia in urania at low temperature, irradiation could have an important impact on the effective solubility of zirconium in urania.

The diffusion process can also considerably slow down the segregation mechanism. The formation of a separate phase enriched in zirconium at the grain boundaries requires the cationic diffusion towards these sites. There are apparently no data for diffusion of zirconium in urania. Yashima et al. [30] estimated, on the basis of experimental information, the duration for Zr^{4+} to diffuse over a distance of 1 μm to be 120 days at 1473 K in CeO_2 which has a similar crystalline structure to UO_2. This implies a diffusion coefficient for zirconium $D_{Zr} \sim 10^{-19}$ m^2 s^{-1}. For a typical irradiated UO_2 grain of diameter, $d_g = 20$ μm, it would mean a typical duration (t) for a zirconium FP atom created at the centre of the grain to reach the grain boundary equal to $t = 0.25\, d_g^2/D_{Zr}$, i.e., 12 000 days, which is approximately 60 times the duration of the irradiation period of [9]. This means that the sluggish diffusion of zirconium in fuel should therefore prevent significant formation of zirconate compounds.

Another mechanism able to limit the zirconium segregation at the grain boundaries of irradiated fuel has been recently assumed by Stanek et al. [31] who showed that the segregation energy of different cations (Zr^{4+} in particular) in UO_2 strongly depends on the surface on which the segregation is proceeding. It was shown that zirconium can only segregate on the (1 0 0) surface which is not assumed to dominate in UO_2 [32].

In irradiated fuel, the behaviour of zirconium must be apprehended by considering both solubility and diffusivity aspects at least at low temperature (<1500 K). The assumption of thermodynamic equilibrium at low temperatures (for instance as applied at 1200 K in [9–11] or at 1450 K here with the MEPHISTA calculation) for the description of its behaviour is probably ungrounded. A model considering both solubility and diffusivity aspects (as in the MFPR approach) implies an apparent higher solubility of zirconia in irradiated urania. Some microanalyses performed on irradiated UO_2-coated particles with very high burn-ups (50% FIMA) at temperatures about 1573 K [33] effectively confirm this assumption since 7%wt. zirconium was measured in the fuel whereas the true thermodynamic solubility is lower [34].

At high burn-up, longer irradiation times should favour zirconium diffusion from the grain to the grain boundaries and then formation of zirconate-type phases. At 10% FIMA (as shown by the MFPR calculation, Table 2), irradiation time is, nevertheless, not long enough to permit significant formation of these phases considering the very-low diffusion coefficient of zirconium in fuel. The experimental work of Sato et al. [35] where the radial distribution of zirconate barium precipitates by X-ray microanalysis along the radius of irradiated fuels (of burn-up to 13.3% FIMA) was determined showed that zirconium (and barium) did not precipitate near the cladding where the temperature was in the interval 1073–1273 K, i.e., in agreement with the MFPR predictions for the fuel kernel of the TRISO particle of similar burn up (10%).

At higher temperature (1700 K), the reduction of uranate amounts is more significant and there is a preferential trapping of barium and strontium in zirconates ($BaZrO_3$ and $SrZrO_3$). This is mainly due to the increase of the zirconium diffusivity (one order of magnitude) and obviously to the higher thermodynamic

stability of these compounds relative to that of uranates. The microanalyses [33] performed on irradiated UO_2-coated particle at an intermediate temperature (about 1573 K) effectively showed that a part of the zirconium was associated with the perovskyte phase with barium and strontium.

In the microanalyses performed on TRISO particles [9,33], it is observed that strontium and barium do not behave exactly similarly. They can be associated in the perovskyte phase (as previously discussed) at the grain boundaries if zirconium has diffused [33] or found in the UO_2 matrix (higher solubility for strontium than for barium) [33] but only some part of barium is released from the kernel to the buffer, at least above 1573 K [9,33]. Thermodynamic calculations (Fig. 4) reproducing the experimental conditions of [9] (4% FIMA, 1700 K) show that BaO is the most probable volatile species for barium (in agreement with the observations in [9]) at the oxygen potential calculated by MFPR (-425 kJ mol^{-1}).

3.2.2. Caesium behaviour

The MFPR calculations evidence a relatively different speciation for caesium between 1450 and 1700 K. Usually caesium is expected to be found in precipitates since it is lowly soluble in fresh UO_2 (0.07 wt.% of Cs in UO_2 at 2173 K in [25]). In irradiated UO_2 fuel at slightly lower temperature (i.e. between 1973 and 2173 K), some experimental observations seem to evidence the same thermodynamic behaviour [36] Ab initio calculations [42] have recently shown that incorporation of caesium in slightly hyperstoichiometric UO_{2+x} could be favoured in case of increase of uranium vacancy concentration which happens in fuel submitted to irradiation (exactly as for zirconium, as previously discussed). Nevertheless, incorporation (or solution) energy of caesium in uranium vacancy [42] is considerably lower than for zirconium [37]. For that reason, its behaviour is expected to be different from that of zirconium. In the calculations at 4% FIMA (Tables 1 and 3), caesium is effectively found in oxide ternary phases, mainly in molybdate phase (Cs_2MoO_4) at 1700 K whereas it is trapped in uranate-type compounds (Cs_2UO_4) at lower temperature (1450 K). The difference of chemical forms of caesium between low and high temperature (uranate versus molybdate) in the calculations is attributed to the higher oxygen potential reached at 1700 K (-425 kJ mol^{-1}) which enhances the depletion of the metallic precipitates in molybdenum and then the correlative increase of Cs_2MoO_4 amount. The cationic diffusion inside the fuel matrix is not, in this case, the limiting process at low temperature since the diffusion coefficient for molybdenum is equal to 5×10^{-16} m^2 s^{-1} in MFPR in accordance with [38], i.e., 5000 times the value of the diffusion coefficient of zirconium.

Nevertheless, an important finding of the Minato's experimental study is the presence of caesium in the carbon buffer layer at 1700 K, i.e., released from the UO_2 kernel. In the MFPR calculation (Table 3), only a very minor part of caesium (0.2%) is released at this temperature and the main part caesium is trapped in ternary oxide compounds (mainly molybdate) which are, on the contrary, not detected in the microanalyses performed by Minato et al. [9].

It must be stressed that if caesium molybdate formation is usually thermodynamically favoured in the absence of any limitations by kinetics or Mo supply under oxygen potential and temperature of fuels of PWR, this compound, as far as the authors are aware, was never detected in PWR irradiated UO_2 fuels. The HTR conditions are expected to be much more less favourable for the formation of this compound in TRISO fuel kernels taking into account, firstly the carbon rich environment which tends to reduce the oxygen potential and secondly, the initial enrichment (e.g. 8% in the Minato's tests [9]) which contributes to have an irradiation process less oxidising. The possibility of forming Cs_2O and MoO_x, constituent oxides of caesium molybdate, is expected then to be strongly reduced. If the trapping of molybdenum in metallic inclusions, in agreement with the observations in [9], is considered as the most probable situation, formation of caesium molybdate should proceed by another mean. McFarlane et al. [39] assumed a possible reaction between CsI, UO_{2+x} ($x = 0.1$) and *metallic* molybdenum leading to the formation of Cs_2MoO_4. They investigated this reaction between 1100 and 1500 K and it was shown to only progress to a small extent, most CsI remaining undissociated.

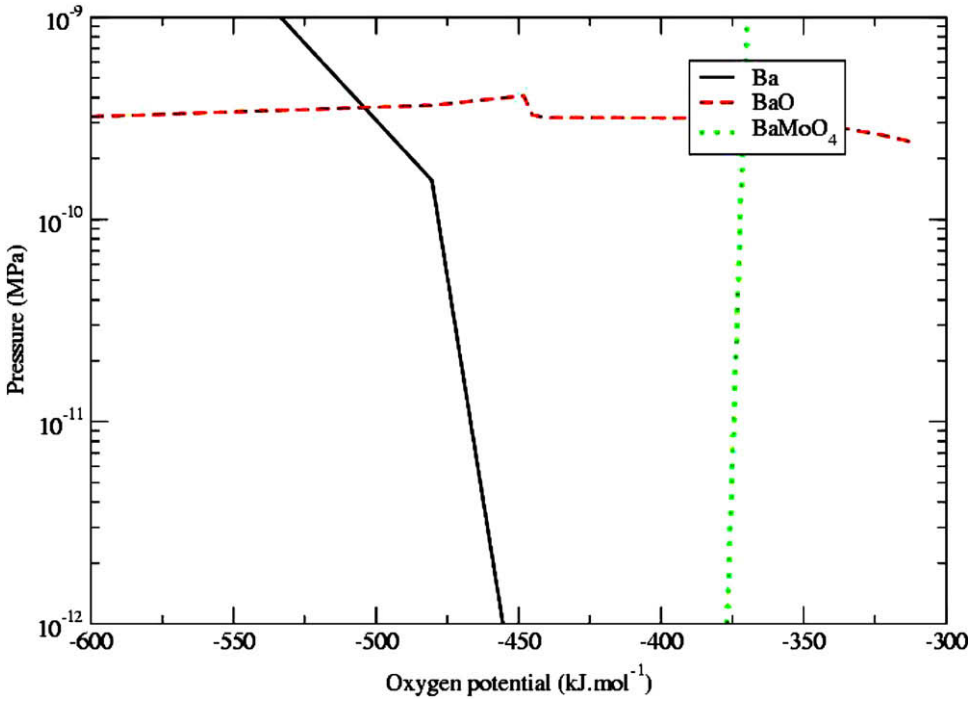

Fig. 4. Thermodynamic calculations of pressures of different compounds including Ba as a function of oxygen potential (4% FIMA, 1700 K).

Observations by Walker et al. [36] showed that release of caesium in irradiated UO_2 fuel (<6.5% FIMA) under post-irradiation *anneal* conditions above 1473 K is similar to xenon behaviour. The described mechanism of release is governed by the degree to escape tunnels at the grain boundaries have developed during irradiation. The MFPR calculations (see following sections) foresee the creation of interconnected porosities in the fuel kernel microstructure under irradiation regime leading to significant release of xenon at 1700 K (but also at 1450 K). The fuel microstructure (as predicted by MFPR) could then effectively provide escape routes for caesium for reaching the carbon buffer layer. For kernel UO_2 under irradiation regime, the mechanism for caesium to reach these routes depends both on temperature and irradiation conditions:

- at high temperature (1700 K), it is expected that the atomic caesium and xenon diffusion assisted by thermally created defects dominates [40]. Crocombette [41] showed by means of ab initio calculations, that uranium vacancy is the more energetically favourable site in UO_{2+x} for trapping Kr. The incorporation of caesium in UO_{2+x} investigated by similar calculations techniques [42] is predicted to the most favourable in the uranium vacancy sites. On this basis, similar mechanisms of diffusion for caesium and xenon can be assumed as the observations by Walker et al. [36] seemed to indicate.
- at lower temperature (1450 K), it is expected that the atomic caesium and xenon diffusion induced by irradiation should dominate [40]. No experimental observations are available but 'recirculation' of caesium atoms in fuel (not actually modelled in MFPR) should be similar to the recirculation fission gases (see following sections for the description of the mechanism) and then leads, as for xenon, caesium to reach grain boundaries.

From this analysis, it can be only concluded that conditions in terms of oxygen potential and fuel microstructure (open porosities) are likely combined to favour caesium release from fuel kernel towards the carbon buffer layer of the particle. This is the situation at moderate burn-up. At higher burn-up for which the oxygen potential is expected to be higher, some part of caesium could be trapped in oxide ternary phases in the fuel kernel. Microanalyses performed by Kleykamp on irradiated coated particles (50% FIMA, 1573 K) [33] effectively seem to indicate that part of caesium is present in the $(Cs,Ba,Sr)(U,Zr,Mo)O_3$ perovskyte phase. It must be noticed that the examined particles in [33] were initially very highly enriched (90%) and then different from the point of view of the evolution of the oxygen potential under irradiation. For that reason, these microanalyses are only indicative of what it may happen at high burn-up in the TRISO fuel particles for the actual VHTR technology.

Once in the buffer, caesium may react with carbon. The MEPHISTA thermodynamic calculation indicates that, for a value of oxygen potential equal to $-455\ kJ\ mol^{-1}$, caesium and graphite effectively react, at 1450 K, to form caesium carbide ($C_{60}Cs$). The threshold oxygen potential for the formation of Cs_2MoO_4 out of $C_{60}Cs$, as calculated by MEPHISTA is $-385\ kJ\ mol^{-1}$ at 1450 K (Fig. 5). It is interesting to underscore that it is not foreseen formation of oxide forms of caesium (uranate or zirconate) for practically all the interval range of oxygen potentials given in [20], i.e., between -380 and $-500\ kJ\ mol^{-1}$. At temperatures higher than 1500 K, the caesium carbide compounds are assumed to be no more stable in MEPHISTA. At temperatures higher than 1500 K, caesium zirconate Cs_2ZrO_3 becomes the stable compound for caesium in the condensed state at low oxygen potentials.

The question of the stability of the C_nCs compounds at temperatures higher than 1100 K is an important concern. At nominal temperature (1450 K) caesium may be released and associated with carbon of the buffer layer to form compounds. These compounds, if they are not stable with increasing of temperature, may become a potential source of caesium release. The thermodynamic properties of these compounds, C_nCs ($n = 8$, 10, 24, 36, 48, 60) in MEPHISTA are derived from vapour pressures measured between 670 and 1070 K [43,44]. There is no data at higher temperatures as mentioned in different reviews [45,46]. It was only shown that caesium-graphite compounds are not stable at 923 K under vacuum and decompose to give caesium vapour and

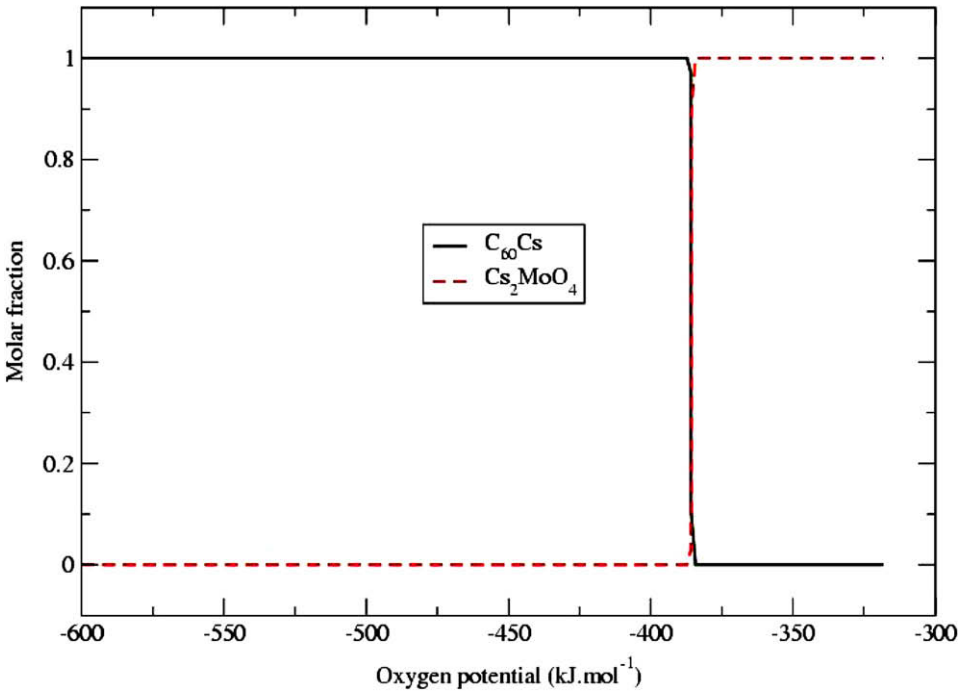

Fig. 5. Cs distribution between the different condensed phases as a function of oxygen potential at 1450 K.

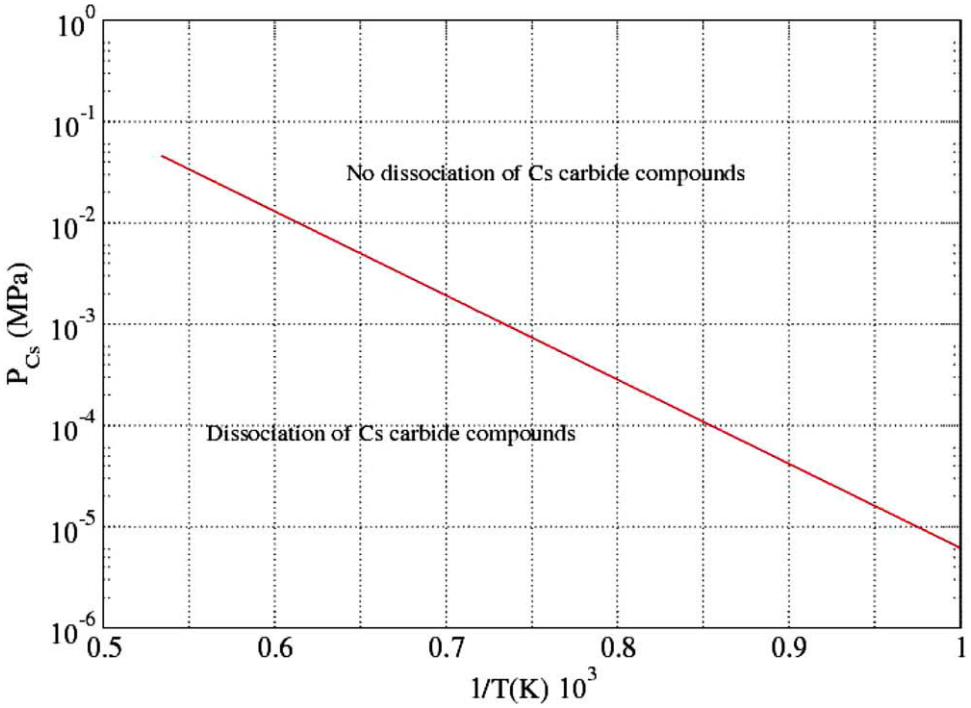

Fig. 6. Threshold pressure for the reaction between caesium and graphite [Eq. (1)].

graphite [47]. A method was developed [48] for estimating the conditions under which graphite reacts with caesium in HTR conditions (high temperatures and low caesium pressures) to form compounds. The following expression is given for the threshold partial pressure of caesium (in Pa), at any temperature (in K), below which no reaction occurs between caesium and graphite (Fig. 6):

$$P(\mathrm{Cs}) = 10^5 \ \exp(-158992/RT + 78.34/R) \qquad (1)$$

with R, the ideal gas constant (J mol^{-1} K^{-1}).

Indicative comparisons between this threshold partial pressure of caesium and the thermodynamic partial pressure of caesium within the particle have been performed at 4% FIMA and 10% FIMA. In these comparisons, it is assumed that caesium is totally released. It means that caesium is not trapped in any ternary phases (molybdate or zirconate) in the kernel. Fig. 7 indicates that, for 4% and 10% FIMA, caesium carbide compounds would be formed at 1450 K. In contrast caesium would be chemisorbed in graphite in accidental conditions (1873 K).

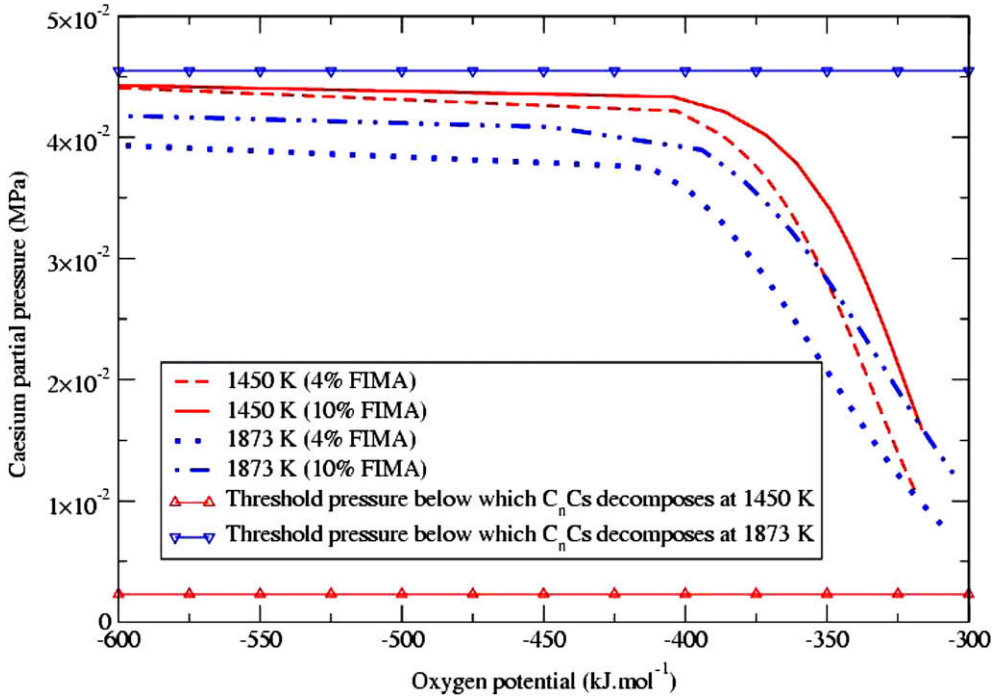

Fig. 7. Comparison between threshold pressure for the reaction between caesium and graphite and thermodynamic partial pressure of caesium within the particle.

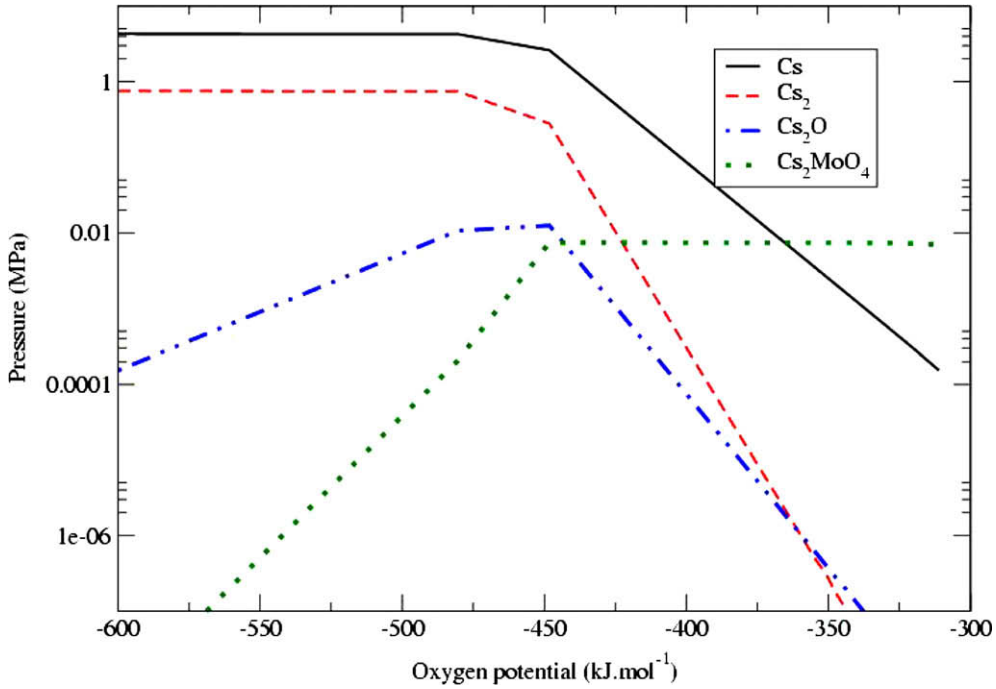

Fig. 8. Thermodynamic calculations of pressures of different compounds including Cs as a function of oxygen potential (4% FIMA, 1700 K).

Coming back to the Minato's observations, in Fig. 8, the calculated thermodynamic pressures of the different species including caesium at 1700 K with a chemical inventory corresponding to 4% FIMA are plotted. It shows, as already noted in [10], that as the oxygen potential increases, the pressure of caesium decreases. The presence of caesium in the buffer layer at 1700 K [9] consequently pleads for a *relatively* low oxygen potential in the particle. The threshold of oxygen potential (~ -450 kJ mol^{-1}) from which the caesium pressure begin to decrease (Fig. 8) depends on the thermodynamic description of the condensed phases in MEPHISTA. The calculated threshold of -450 kJ mol^{-1} is linked to the formation of Cs_2MoO_4 out of Cs_2ZrO_3. If thermodynamic properties of carbide compounds are extrapolated in order to stabilise them up to 1700 K, the threshold is shifted to -340 kJ mol^{-1} and corresponds to the formation of Cs_2MoO_4 out of $C_{60}Cs$. In any case, for an oxygen value presumably lower than -425 kJ mol^{-1}, caesium would be released in agreement with Minato's observations.

3.2.3. Ruthenium and molybdenum behaviour

Ruthenium and molybdenum (in case of release from the fuel kernel), as caesium, could present a particular speciation, in respect to the PWR UO_2, due the carbon rich environment. At low

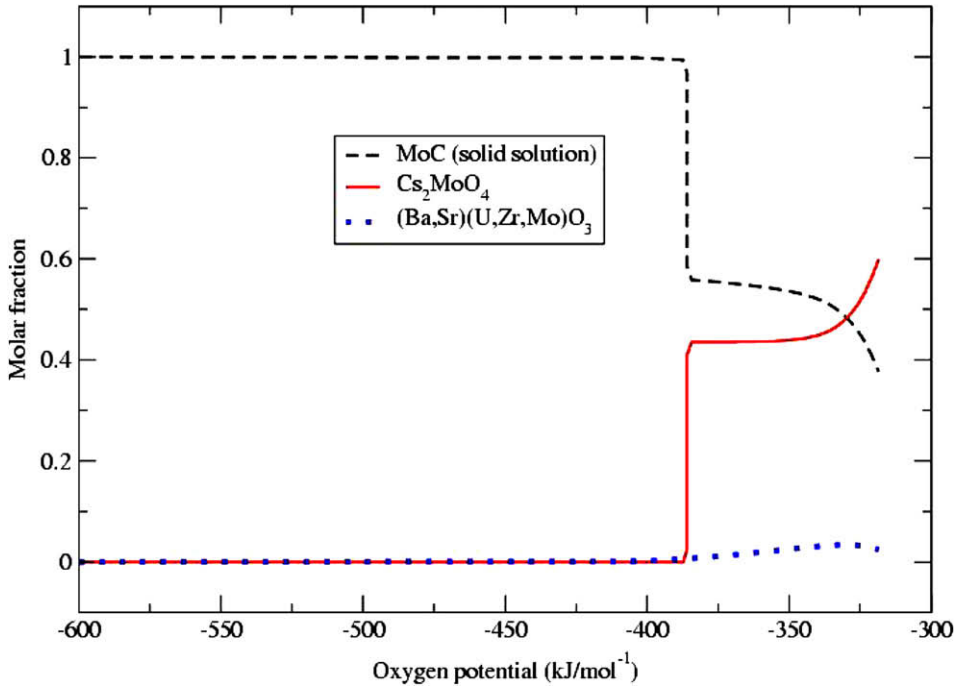

Fig. 9. Mo distribution between the different condensed phases as a function of oxygen potential at 1450 K.

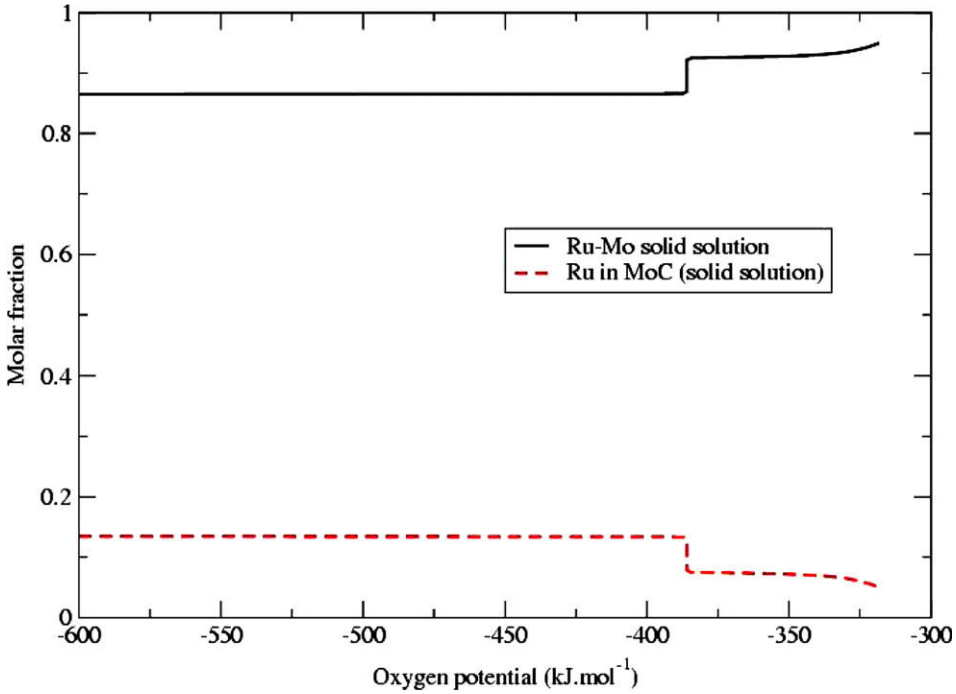

Fig. 10. Ru distribution between the different condensed phases as a function of oxygen potential at 1450 K.

oxygen potential (i.e., −450 kJ mol^{-1}), at 1450 K, thermodynamic calculations show that:

- molybdenum may form carbide (Fig. 9). No detection of such precipitates was mentioned in the analyses of the buffer in [9].
- a small part of ruthenium may associate to molybdenum carbide (solid solution) whereas the main part remains in the metallic precipitates Ru–Mo (Fig. 10). The microanalyses performed on irradiated UO_2-coated particles with very high burn-up (50% FIMA) at temperatures about 1573 K [33] effectively showed association between ruthenium and molybdenum in the carbon buffer layer. These associations have to be confirmed for TRISO particles more representative in terms of burn-up.

4. Fission-gas behaviour and fuel microstructure

The case of the UO_2 kernel in TRISO-coated particles is unusual compared to PWR UO_2 fuel because the fission rate and the temperature are very high. Fuel microstructural characteristics and fission-gas behaviour may then evolve in different ways for TRISO-coated particles. These items, in particular the fuel microstructure evolution, are usually not investigated in the post-irradiation examinations performed on TRISO particles. They play an important role in the release mechanisms of FP in nominal regimes and in the case of accident conditions since they determine the escape routes for fission products. MFPR calculations allow significant insights into these subjects.

4.1. Fission-gas behaviour

From PWR UO_2 fuel experience, a general knowledge of fission-gas behaviour is available, described in [49]. The fission gases are of very low solubility and form bubbles in the grain. Both gas atoms and (in a very much lesser extend) bubbles migrate to the grain boundaries where gas porosities are created and grow by atoms and vacancies capture or by coalescence on the grain face. After sufficient growth, the face bubbles are able to form interconnected porosities leading to the further growth of edge bubbles which, after reaching a critical swelling value, can form an open path to the fuel free volumes. Such a percolation-type mechanism [50] is implemented in the MFPR code and reproduces correctly the main trends of the gas behaviour in irradiated UO_2 fuel for PWR.

In the UO_2 kernel of TRISO-coated particles, both fission rate and temperature are significantly higher which induces different fission-gases behaviour. The higher temperature reached in these particles leads to an increase in the thermal gas atoms diffusivity which would lead to higher gas concentration at grain boundaries. This would also increase the coalescence of the face bubbles and gas atoms capture by bubbles [49]. On the other hand, the irradiation effects additionally increase gas atoms mobility and induce very high gas atom re-solution from bubbles in the grain and at grain boundaries. In the grain the re-solution process limits significantly gas trapping by bubbles. At the grain boundary, the re-solution from bubbles on grain faces give 'circulation' of gas atoms collected by growing intergranular bubbles from the grain face and then returned back (by the re-solution process) into the grain matrix, making intergranular bubbles much less effective sinks for gas atoms, since it decreases their growth (i.e., approaching a balance among absorbed and re-emitted atoms). Thus a continuously increasing fraction of the source term flux (i.e., diffusion flux from grain to grain face) is eventually transported to grain edges. In particular, this permits a possible gas release from fuel when the grain-face coverage is far below the saturation value (at which interlinkage of face bubbles occurs generally taken as 50%).

Such models describing irradiation effects are implemented in MFPR. Fig. 11 shows the results obtained for high fission rate with high temperature (1700 K) and lower temperature (1450 K). In any case the gas release is very significant, in agreement with some preliminary experimental observations [51]. The gas release is always significant and increased in case of high temperature (because of thermal effects in atoms mobility). As shown by Fig. 12, the face bubble size remains limited (<1 μm) and gas release with a very-low grain-face coverage fraction (20% at 1700 K and ~6% at 1400 K) is possible. Nevertheless, one must be careful with the validity of re-solution models which are still in discussion (see

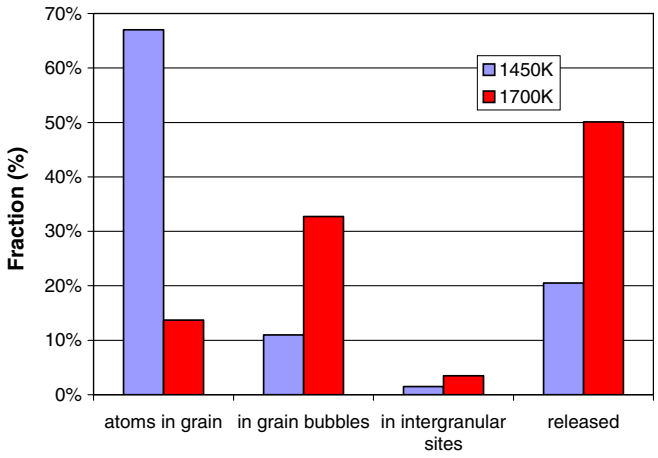

Fig. 11. Fission-gas (Xe) location in UO_2 kernel (at 1450 and 1700 K and 4% FIMA).

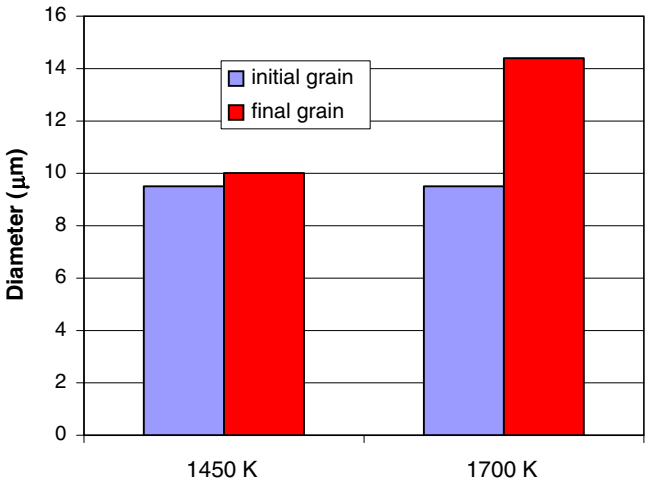

Fig. 13. Grain size evolution for UO_2 kernel (at 1450 and 1700 K and 4% FIMA).

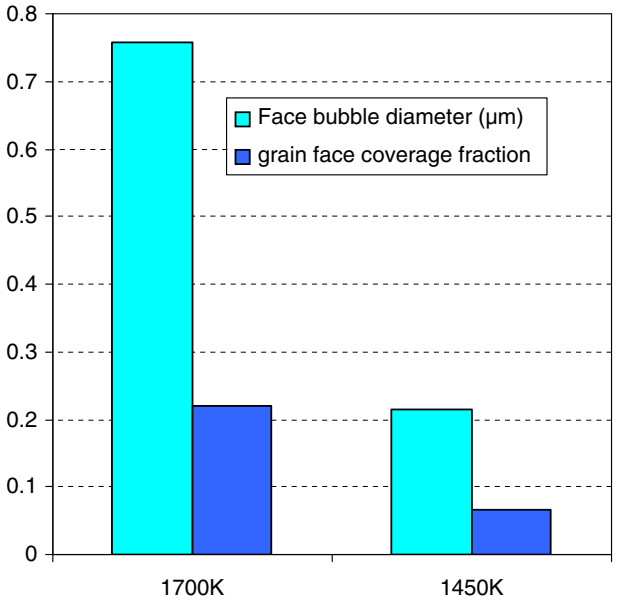

Fig. 12. Face bubble diameter and grain-face coverage fraction for UO_2 kernel (at 1450 and 1700 K and 4% FIMA).

[52] for re-solution in the grain). Additional calculations with different models for gas re-solution from bubbles (reducing this effect) were performed and gave also significant release but this time with interconnection of face bubbles.

The thermodynamic analysis (see Section 2), assuming isochoric conditions, predicts that total pressure may approach 30 MPa. According to the work by Kashibe and Katsumi [53], this pressure is insufficient to have a major influence on fission-gas release at the relatively low burn-ups of their experiments (~4% FIMA). Furthermore, the release mechanism in the HTR conditions involves, according to our predictions, release via interconnected edge bubbles without interconnection of face bubbles. This may reduce the possible effect of particle pressurization on the release. Hence, a strong effect of the pressure on the release is not expected.

4.2. Fuel microstructure

As said above, the high fission rate leads to strong gas atoms re-solution from bubbles. Bubble size (grain face and edge) might then be strongly limited. Association of limited intergranular bubbles size and high temperature is able to give significant grain growth [54]. In our case, as shown in Fig. 13, such grain growth is foreseen at 1700 K. In [51], a significant increase of the grain size was observed at 1500 K.

It must be noted that the behaviour of intergranular porosities determines the grain size evolution. At high temperature (but also high fission rate and strong re-solution) growth of intergranular bubbles might be important. In MFPR, only coalescence of face bubbles by random migration is considered which could be a problem at high temperature where coalescence by growth and impingement might be effective [55]. Such model will be implemented in the future version of MFPR but it could be anticipated that significant face bubble growth occurred (namely at 1700 K) in closer qualitative agreement with experimental observations in [51] and to a decrease of grain growth when these large porosities are created.

An additional very important effect of the high fission rate is to increase the concentration of point and extended defects. At high temperature (Fig. 14) the relative (to the thermal equilibrium value) vacancy concentration evolution together with their two main sink strength terms in grain bubbles and dislocation as a function of burn-up is plotted (other sink terms are of minor importance). From Fig. 14, one must note that the vacancy concentration remains higher than the thermal equilibrium value:

- at the first stage of the irradiation process (up to 0.5% FIMA) the dislocation concentration is relatively low. The vacancy concentration can then freely increase and the grain bubble concentration also increases. Indeed the behaviour of grain bubbles is strongly associated with vacancy concentration. In the case of steady-state irradiation conditions, the bubble nucleation factor is proportional to the probability that a vacancy is located in a certain position (collision of two atoms) and therefore to the vacancy concentration.
- at higher burn-up (>0.5% FIMA), the increase of the extended defects and the grain bubbles (Fig. 12) tends to limit, by trapping, the vacancy concentration which in turn impacts the bubble grain concentration. It leads to the well known saturation of the grain bubble concentration evolution.

Dislocations are generated under irradiation in the form of di-interstitial clusters and continuously grow by absorption/emission of point defects in two types, dislocation loops and dislocation network. A simple approach is developed by considering bi-modal distribution of loops, their evolution and transformation into

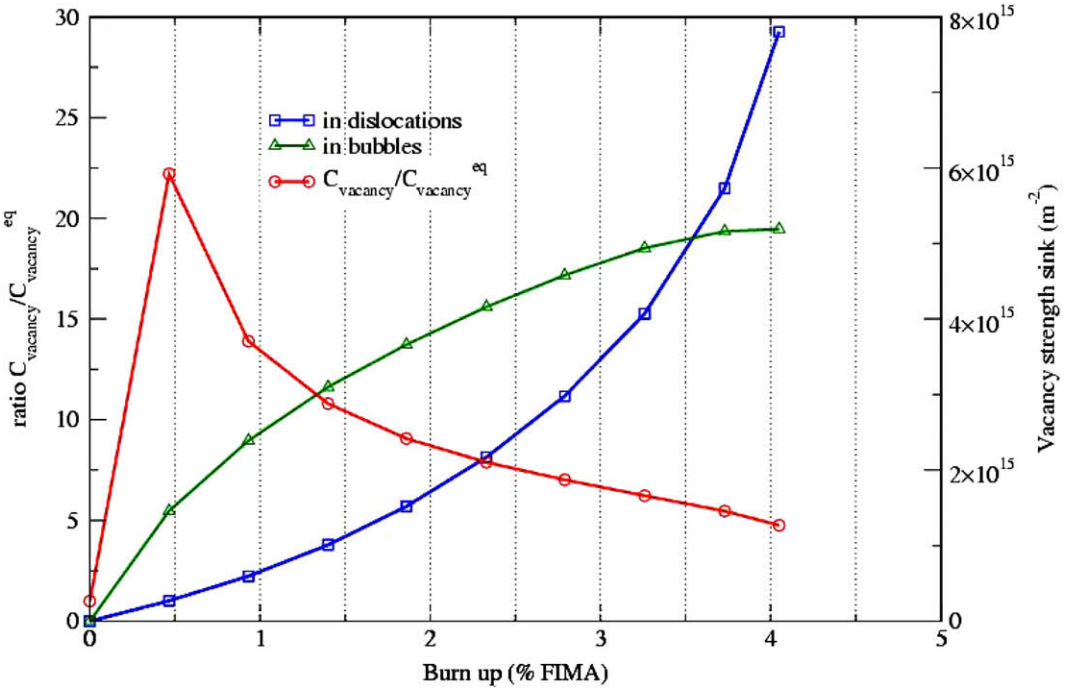

Fig. 14. Vacancy, grain bubble and dislocation concentrations (1700 K).

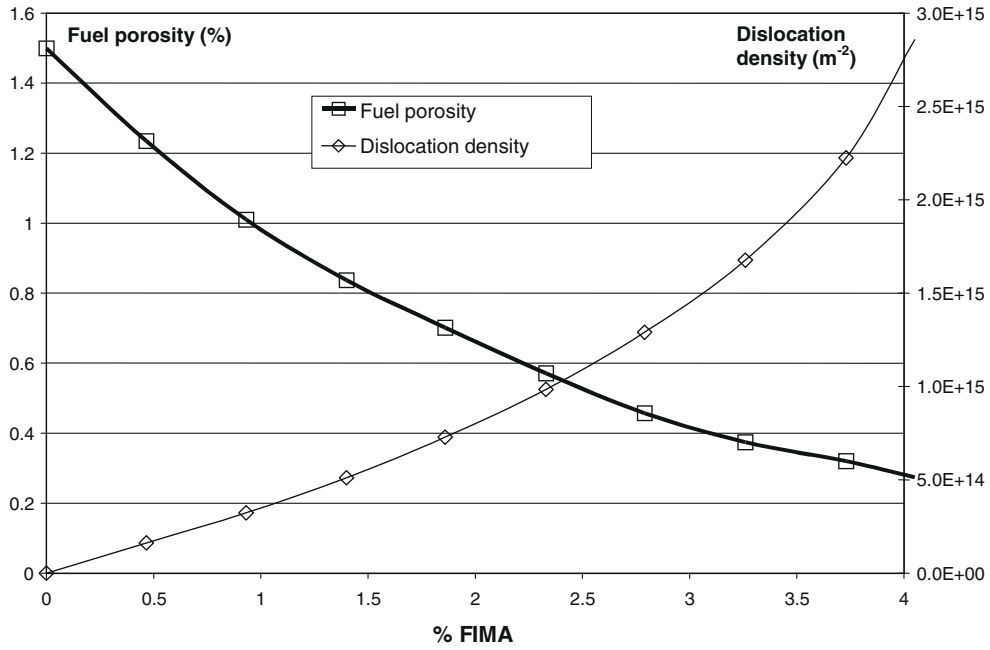

Fig. 15. Dislocation density and fuel porosity (1700 K).

dislocation network [56]. The results for high temperature are given in Fig. 15, rather similar to those obtained at lower temperature. The value for dislocation density is very high. As observed in [57] at about 900 K, tangled dislocation networks with low-angle grain boundaries might form by accumulation of dislocations when dislocation density attains $\sim 6 \times 10^{14}\ m^{-2}$ in fuel of typical burn-up of 5% FIMA. At higher burn-up, there is transition from low-angle to large-angle cells occurring in the range of dislocation density from $\sim 6 \times 10^{14}$ to $\sim 10^{15}\ m^{-2}$ which can be defined as a possible criterion for evolution to sub-divided grains with high-angle boundaries postulated as the nucleus for the re-crystallization of fuel [58]. Such effect could be foreseen in our case.

Nevertheless, one must take care with the complex behaviour of dislocations at high temperature. An additional mechanisms (unaccounted in the current model) leading to the dislocation density reduction operates at high temperatures (e.g. mutual annihilation of dislocations, release from grains due to sliding under thermal stresses, etc.). A dislocation sliding mechanism (with some activation energy at the initial static recovery, which is the energy for dislocation annihilation by glide or cross-slip) might operate at high temperature inducing annihilation. The consequence is usually an increase of the material ductility. On the contrary, at low temperature, the dislocations tend to be locked and move with difficulty (brittle behaviour). Since the ductile behaviour of (fresh)

UO_2 prevails at temperatures above ~1473 K [59], the current dislocation model cannot be applied with confidence to the high-temperature range.

Recent modifications in the MFPR approach taking into account non-equilibrium vacancy concentration on dislocation and its dependence on elastic energy and stacking fault energy of dislocation loop, showed a noticeable decrease of the dislocation density at 1300–1400 K (nominal conditions of HTR) and then no restructuring at this temperature up to 10% FIMA in agreement with recent experimental observations [60], also confirmed by more recent observations of [51] where no restructuring was observed at 1300 K for very-high burn-up fuel, around 11%FIMA.

5. Conclusion

Based on comparison with experimental data, the physico-chemical composition of irradiated TRISO-coated fuel particles has been investigated using the non-ideal solution thermodynamic database MEPHISTA and the mechanistic fuel-analysis code MFPR. This study had the dual objective of developing the understanding of FP behaviour within such particles while honing the analysis capabilities of these approaches in the special conditions of HTR fuel.

An initial conclusion concerns the analysis approaches themselves. They were developed for specific PWR applications and it has been found that they have certain shortcomings with respect to HTR conditions (i.e., the dislocation model in MFPR, limited number of FPs in MEPHISTA). Due to these limitations, an important item identified as a safety concern relates to silver (^{110m}Ag) migration and speciation through the different coatings [61,62] that could not be studied in the present paper.

Nevertheless, these shortcomings were offset to a great extent by the complementary nature of the MEPHISTA and MFPR analyses. The following main conclusions can be identified with respect to irradiated TRISO fuel:

- the relatively low oxygen potential within the fuel particles with respect to PWR fuel leads to chemical speciation that is not typical of PWR fuels, e.g., the relatively volatile behaviour of barium;
- the safety-critical FP caesium is released from the urania kernel but the buffer and pyrolytic-carbon coatings form an important chemical barrier to further migration (i.e., formation of carbides);
- significant (~20% or more) release of fission gases from the urania kernel is expected even in nominal conditions;
- for fuel microstructure, significant grain growth and porosity coalescence might be expected. Despite the very significant irradiation-induced damage, the high temperature will tend to decrease dislocation density and probably avoid fuel recrystallisation.

Looking to the future, additional data from micro-characterizations of TRISO particles would be extremely valuable. This is particularly true with respect to confirming the absence of ternary phases as advanced in [9]. Further work is planned in this direction. The next step will be analysis of the HFR-EU1bis test performed within the RAPHAEL Project [51].

Acknowledgments

The authors would like to acknowledge B. Cheynet and E. Fischer (THERMODATA/INPG/CNRS) for their contribution to this work. M.S. Veshchunov (IBRAE) is also thanked for the fruitful discussions about fuel microstructure evolution under irradiation.

References

[1] D. Greneche, W.J. Szymczak, Nucl. Eng. Des. 236 (5–6) (2006) 635.
[2] E. Proksch, A. Strigl, H. Nabielek, J. Nucl. Mater. 107 (1982) 280.
[3] M. Phélip, F. Charollais, S. Shihab, K. Bakker, P. Guillermier, P. Obry, T. Abram, M.A. Fütterer, E. Toscano, H. Werner, M. Kissane, High-temperature Reactor Fuel Technology in the European Projects HTR-F1 and RAPHAEL, in: Proceedings of the Third International Topical Meeting on High Temperature Reactor Technology, 1–4 October 2006, Johannesburg, South Africa, 2006.
[4] K. Minato, T. Ogawa, K. Fukuda, H. Sekino, H. Miyanishi, S. Kado, I. Takahashi, J. Nucl. Mater. 202 (1993) 47.
[5] D.R. Olander, Fundamental Aspects of Nuclear Reactor Fuel Elements, Report TID-26711-P1. Technical Information Center, US Department of Energy, 1976.
[6] M.S. Veshchunov, V. Ozrin, V. Shestak, V. Tarasov, R. Dubourg, G. Nicaise, Nucl. Eng. Des. 236 (2006) 179.
[7] B. Cheynet, E. Fischer, MEPHISTA: A Thermodynamic Database for New Generation Nuclear Fuels. <http://hal.archives-ouvertes.fr/hal-00222025/fr/>.
[8] L. Kaufman, H. Bernstein, Computer Calculation of Phase Diagrams with Special Reference to Refractory Metals, Academic Press, New York, 1970.
[9] K. Minato, T. Ogawa, K. Fukuda, M. Shimizu, Y. Tayama, I. Takahashi, J. Nucl. Mater. 208 (1994) 266.
[10] R.P.C. Schram, E.H.P. Cordfundke, A.I. Van Heek, High-temperature Reactor Developments in Netherlands, in: Proceedings of the Third JAERI Symposium on HTGR Technologies, 15–16 February 1996, Japan, 1996.
[11] J.C. Dumas, J.P. Piron, S. Chatain, C. Guéneau, Adv. Sci. Technol. 45 (2006) 1944.
[12] J.H. Davies, F.T. Ewart, J. Nucl. Mater. 41 (1971) 143.
[13] C.T. Walker, V.V. Rondinella, D. Papaioannou, S. Van Winckel, W. Goll, R. Manzel, J. Nucl. Mater. 345 (2005) 192.
[14] J. Spino, P. Peerani, J. Nucl. Mater. 375 (2008) 8.
[15] P.Y. Chevalier, E. Fischer, J. Nucl. Mater. 288 (2001) 100.
[16] P.Y. Chevalier, E. Fischer, B. Cheynet, J. Nucl. Mater. 303 (2002) 1.
[17] P.E. Potter, J. Nucl. Mater. 42 (1972) 1.
[18] S. Gossé, C. Guéneau, C. Chatillon, S. Chatain, J. Nucl. Mater. 352 (2006) 13.
[19] R.N. Morris, D.A. Petti, D.A. Powers, B.E. Boyack, TRISO-Coated Particle Fuel Phenomenon Identification and Ranking Tables (PIRTs) for Fission Product Transport Due to Manufacturing, Operations, and Accidents, US NRC Report NUREG/CR-6844, vol. 1, 2004.
[20] T.B. Lindemer, H.J. de Nordwall, An Analysis of Chemical Failure of Coated UO_2 and other Oxide Fuels in the High Temperature Gas-Cooled Reactor, Technical Report ORNL-4926. Oak Ridge National Laboratory, 1974.
[21] C. Guéneau, S. Chatain, J.C. Dumas, J. Lechelle, C. Rado, F. Defoort, N. Dupin, B. Sundman, H. Noel, R. Konings FUELBASE: A Thermodynamic Database for Advanced Nuclear Fuels, in: Proceedings of the Third International Topical Meeting on High Temperature Reactor Technology, 1–4 October 2006, Johannesburg, South Africa, 2006.
[22] S. Gossé, C. Guéneau, T. Alpettaz, S. Chatain, C. Chatillon, F. Le Guyadec, Nucl. Eng. Des. 238 (2008) 2866.
[23] L.J. Kaee, Nucl. Technol. 35 (1977) 359.
[24] M. Wagner-Loffler, Nucl. Technol. 35 (1977) 392.
[25] H. Kleykamp, J. Nucl. Mater. 206 (1993) 82.
[26] H. Kleykamp, J.O. Paschoal, R. Pejsa, F. Thummler, J. Nucl. Mater. 130 (1985) 426.
[27] E.H.P. Cordfunke, R.J.M. Konings, J. Nucl. Mater. 152 (1988) 301.
[28] K.A. Romberger, C.F. Baes Jr., H.H. Stone, J. Inorg. Nucl. Chem. 29 (1967) 1619.
[29] R.W. Grimes, C.R.A. Catlow, Philos. Trans. R. Soc. London A 335 (1991) 609.
[30] M. Yashima, H. Takashina, M. Kakihana, M. Yoshimura, J. Am. Ceram. Soc. 77 (1994) 1869.
[31] C.R. Stanek, M.R. Bradford, R.W. Grimes, J. Phys.: Condens. Matter 16 (2004) S2699.
[32] A.A.H. Tan, R.W. Grimes, S. Owens, J. Nucl. Mater. 344 (2005) 13.
[33] H. Kleykamp, Mikrosondenuntersucchungen zum Verhalten der Spaltprodukte in hoch abgebrannten HTR-Brennstoffen, Technical Report KfK-2213, 1975.
[34] P.Y. Chevalier, E. Fischer, B. Cheynet, Calphad 28 (2004) 15.
[35] I. Sato, H. Furuya, T. Arima, K. Idemitsu, K. Yamamoto, J. Nucl. Sci. Technol. 36 (1999) 775.
[36] C.T. Walker, C. Bagger, M. Morgensen, J. Nucl. Mater. 240 (1996) 32.
[37] G. Brillant, A. Pasturel, Phys. Rev. B 77 (2008) 184110.
[38] T.J. Heames, D.A. Williams, N.E. Bixler, A.J. Grimley, C.J. Wheatley, N.A. Johns, P. Domagala, L.W. Dickson, C.A. Alexander, I. Osborn-Lee, S. Zawadzki, J. Rest, A. Mason, R.Y. Lee, VICTORIA: A Mechanistic Model of Radionuclide Behaviour in the Reactor Coolant System Under Severe Accident Conditions, NUREG/CR-5545, SAND90-0756 Rev1 R3, R4, 1992.
[39] J. McFarlane, J.C. LeBlanc, D.G. Owen, High Temperature Chemistry of Molybdenum, Cesium, Iodine and UO_{2+x}, Technical Report AECL-11708, 1996.
[40] J.A. Turnbull, C.A. Friskney, J.R. Findley, F.A. Johnson, A.J. Walter, J. Nucl. Mater. 107 (1982) 168.
[41] J.P. Crocombette, J. Nucl. Mater. 305 (2002) 29.
[42] F. Gupta, Etude du Comportement du Produit de Fission Césium dans le Dioxyde d'Uranium par Méthode ab initio, PhD Thesis, 19 September 2008, Paris XI.
[43] F.J. Salzano, S. Aronson, J. Chem. Phys. 43 (1965) 149.
[44] F.J. Salzano, S. Aronson, J. Chem. Phys. 45 (1966) 2221.
[45] Y.N. Novikov, M.E. Vol'pin, Russ. Chem. Rev. 40 (1971) 733.
[46] J. Sangster, J. Phase Equilib. Diff. 29 (2008) 93.
[47] F.J. Salzano, S. Aronson, J. Chem. Phys. 45 (1965) 1323.

[48] F.J. Salzano, S. Aronson, Nucl. Sci. Eng. 28 (1967) 51.
[49] P. Lösönen, J. Nucl. Mater. 280 (2000) 56.
[50] R.J. White, M.O. Tucker, J. Nucl. Mater. 118 (1983) 1.
[51] S. de Groot, M. Barrachin, R. Dubourg, M. Kissane, Fission Product Behaviour during Irradiation of TRISO Coated Particles: HFR Eu1bis Test, in: Fourth International Topical Meeting on High Temperature Reactor Technology, Washington D.C., September 28–October 1, 2008.
[52] D.R. Olander, D. Wongsawaeng, J. Nucl. Mater. 354 (2006) 94.
[53] S. Kashibe, U. Katsumi, J. Nucl. Sci. Technol. 37 (2000) 530.
[54] M.S. Veshchunov, J. Nucl. Mater. 346 (2005) 208.
[55] M.S. Veshchunov, J. Nucl. Mater. 374 (2008) 44.
[56] M.S. Veshchunov, V.D. Ozrin, V.E. Shestak, V.I. Tarasov, R. Dubourg, G. Nicaise, Modelling of defect structure evolution in irradiated UO_2 fuel in the MFPR code, in: Proceedings 2004 International Meeting on LWR Fuel Performance, September 19–22, Orlando, Florida, USA, American Nuclear Society.
[57] K. Nogita, K. Une, Nucl. Instrum. and Meth. B 91 (1994) 301.
[58] M.S. Veshchunov, R. Dubourg, V. Ozrin, V. Shestak, V. Tarasov, J. Nucl. Mater. 362 (2007) 327.
[59] A.G. Evans, R.W. Davidge, J. Nucl. Mater. 33 (1969) 249.
[60] M. Kinoshita, T. Sonoda, S. Kitajima, A. Sasahara, E. Kolstad, Hj. Matzke, V.V. Rondinella, A.D. Stalios, C.T. Walker, I.LF. Ray, M. Sheindlin, D. Halton, C. Ronchi, High Burnup Rim Project(II) Irradiation and Examination to Investigate Rim-structures Fuel, in: ANS International Topical Meeting on LWR Fuel Behaviour, Park City Utah, USA, April 9–13, 2000.
[61] K. Minato, K. Sawa, T. Koya, T. Tomita, A. Ishikawa, C.A. Baldwin, W.A. Gabbard, C.M. Malone, Nucl. Technol. 131 (2000) 36.
[62] H. Nabielek, P.E. Brown, P. Offermann, Nucl. Technol. 35 (1997) 483.